

Walk away VSP processing of DAS and geophone data at CaMI Field Research Station, Newell County, Alberta

Adriana Gordon and Don C. Lawton

ABSTRACT

As part of the FRS baseline assessment, several Vertical Seismic Profiles were acquired with the intention of testing emerging monitoring techniques such as Distributed Acoustic Sensing (DAS). In this report, we describe the processing flow and discuss the results obtained for a walkaway VSP oriented North-South and centred in the observation well 2. This survey was acquired in July 2017 using two recording systems: fibre optic cables (straight and helical wound fibre) for DAS and a 3C 24-level geophone array. Each section of the report displays a comparison between the straight and helical fibre optic cables and the geophone array. After processing the different datasets, we compared the results of the stacked VSP-CDP transforms with an inline section from a 3D seismic survey crossing through the well. Overall, there is a good correlation between the events in the surface seismic and the VSP-CDP. The CO₂ injection target located at approximately 250 ms is noticeable in each dataset. Nevertheless, there is an apparent discontinuity of the event of interest across the mapped result, particularly for the helical fibre. This assessment shows how DAS measurements seem to be a promising approach for subsurface imaging and continuous monitoring. However, further analysis of DAS is essential to obtain better imaging results, especially for the helical wound fibre optic cable dataset.

INTRODUCTION

The implementation of new technologies at the Field Research Station (FRS) is a key objective of the project as we have noticed in previous reports. One of which is the Distributed Acoustic Sensing (DAS) technique, considered a rapidly developing technology with a number of applications for subsurface monitoring. DAS entails the use of fibre optic cables for seismic sensing along a well or in a horizontal trench. The fibre optic cable is connected to a device called interrogator unit that measures the deformations generated by impinging seismic waves along the fibre (Mateeva et al., 2014). As the interrogator unit sends laser pulses along the fibre, a small part of the laser light is back-scattered due to micro-heterogeneities present in the fibre. When seismic waves reach the fibre, the back-scattered pattern is perturbed and those variations are transformed into seismic measurements (Mateeva et al., 2014).

At the FRS there is installed a loop of fibre optic cable for the study of this emerging technology and to monitor the CO₂ injection program. Straight and Helical Wound Cables (HWC) are deployed in the observation wells in addition to a horizontal trench crossing the site in the NE-SW direction. In this report, we cover the processing flow of a walk away VSP acquired at the FRS utilizing DAS measurements and a geophone array also permanently installed in the Observation Well 2. The intention is to compare the imaging results obtained from DAS and geophones as well as analyzing the differences between the straight and helical wound cables. Also we processed the DAS datasets to resemble the

geophone response. Finally, the results of the different datasets are compared to images from a 3D surface seismic survey of the site.

DATA SET AND PROCESSING FLOW

The Field Research Station (FRS) is located approximately 200 km southeast of Calgary in the Newell County near the town of Brooks (Figure 1). In this study, a North-South walk away VSP was selected for processing among the different surveys acquired in 2017 since it has a consistent number of vibroseis sweeps per source point (6 in this case), which we will refer to as vertical fold. Figure 2 shows the geometry of the line, where source points are coloured in red and the wells are marked with black circles. Although all source offsets were processed, eight particular source points were selected for discussion (blue circles) with respect to the observation well 2 (orange circle). This selection was made to have a consistent comparison regarding the offset from the well on each side of the line.

The seismic source used for the acquisition was an IVI EnviroVibe a with a linear sweep from 10 to 150 Hz over 16 s with 3 s of listen time. The recording systems comprised fibre optic cables with a nominal guage length of 10 m and output trace spacing of 0.25 m and a 24-level 3-component (3C) geophone array covering at depths from 191 to 306 m with a 5 m spacing. Figure 3 displays a schematic of the fibre optic cables deployed at the FRS, and highlighting observation well 2 equipment.

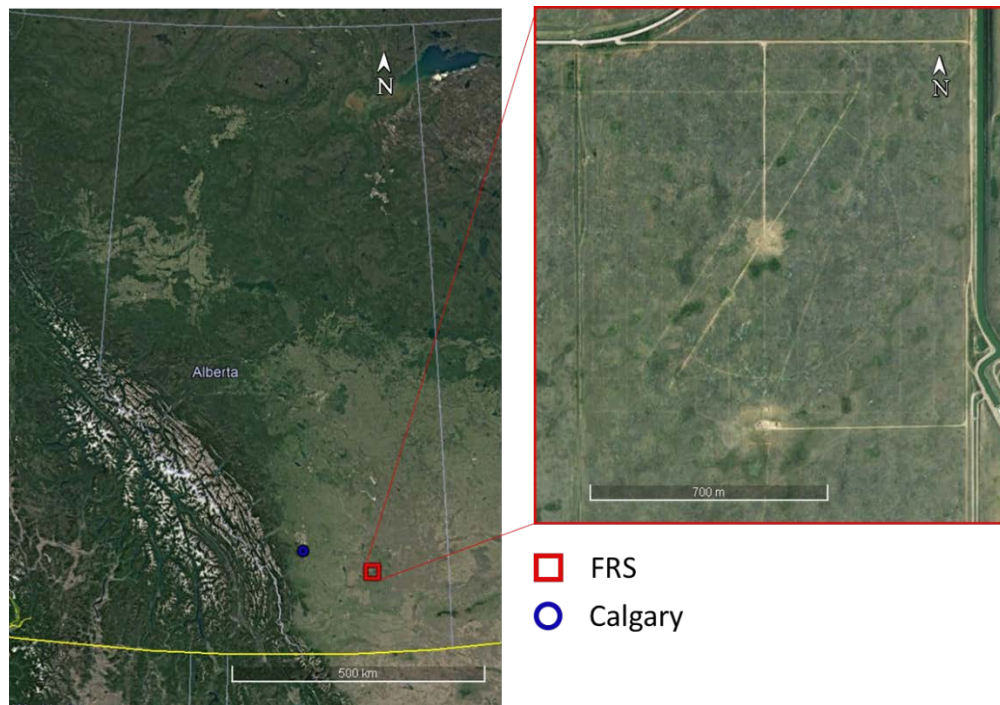


Figure 1. Location of the Field Research Station in Southern Alberta.

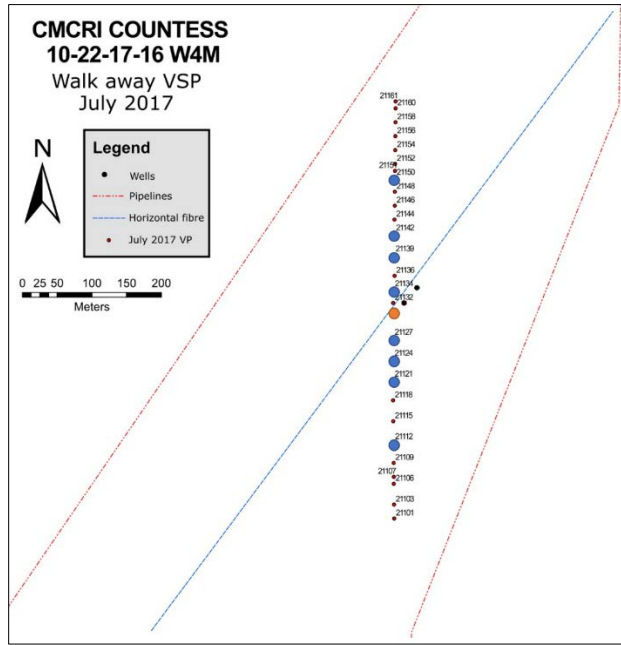


Figure 2. Geometry survey of walk away VSP. Source points in red and wells marked with black circles. Red dashed lines indicate pipelines and the blue line indicate the horizontal trench with fibre optic cables. Blue circles show the source points selected for discussion with respect to the observation well 2 in orange.

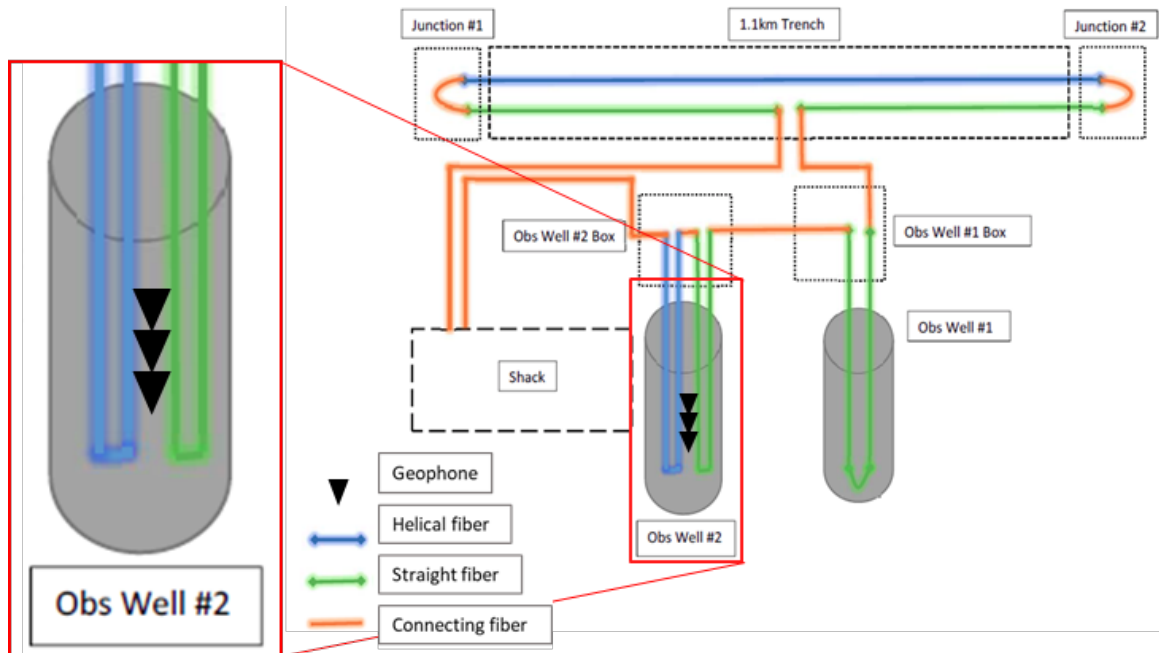


Figure 3. Schematic of the fibre optic cables installed at the FRS. For this report, our focus is on the observation well 2 highlighted with a red rectangle.

A standard processing flow was applied to the datasets which consisted of geometry and first break picking, a depth registration of DAS traces relative to the geophones, wavefield separation through a median filter and an F-K filter for DAS datasets. A deconvolution operator was designed from the downgoing wavefield and applied to the upgoing wavefield, followed by VSP-CDP transform and stack.

In the following sections, we discuss and compare the straight fibre and the helical fibre datasets at each step of the processing flow. The same approach is performed to the integrated DAS datasets with the attempt of transforming the measurements from strain rate to geophone response and therefore have a more comparable assessment. Similarly, the geophone dataset is analyzed by processing the vertical component and the rotated data with the purpose of obtaining a complete analysis of the straight fibre and HWC fibre compared to the multicomponent geophones. The result of each processing step per dataset are presented in the following order: raw DAS, integrated DAS, vertical component geophone and rotated geophone data for each step of the processing flow.

As an example, Figure 4 shows a comparison of the raw DAS datasets (straight and helical fibre) with respect to the geophone vertical component. In general, there is a good identification of downgoing and upgoing waves in each dataset. As the offset increases, the time difference of the first arrivals as well as the arrival of head waves is noticeable in DAS datasets thanks to the full coverage of the fibre in the well. Additionally, the helical wound data seems to have a lower signal to noise ratio than the straight fibre.

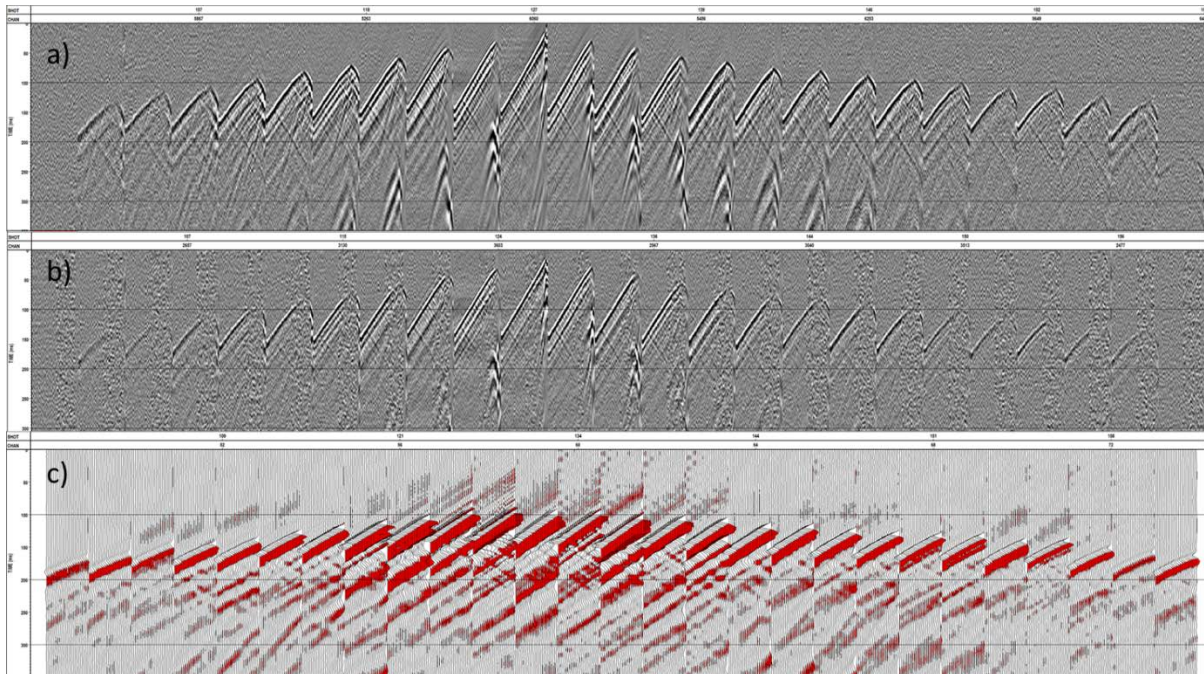


Figure 4. Raw DAS and geophone source gathers of walk away VSP line. a) straight fibre, b) helical fibre and c) geophone vertical component.

Geometry and first break picks

Once the geometry was uploaded, the picking of the first arrivals was completed (Figure 5). Given the number of DAS traces per source gather, there is some scatter in the first break times that can generate discrepancies in the interval velocity profiles. For this reason, a median filter was applied to the first break times for the calculation of the interval velocities.

Knowing that one of the limitations of using DAS is the uncertainty of the exact location in depth of each trace (Mateeva et al. 2014), we carried on a depth registration analysis. For the straight fibre optic cable, the trace spacing is 0.25 m and if the total depth of the observation well 2 is 330 m we would expect to have approximately 1320 traces per source gather. In the case of the helical fibre, there is a higher uncertainty as the trace spacing should be smaller due to the fibre being helically wound on a mandrel. From the first break times we identified the trace with the latest arrival time at a zero offset gather and assuming a total depth of 330 m, we obtained a trace spacing of 0.22 m. The corresponding depth of the DAS traces was updated before continuing with the workflow.

The geophone array has four dead traces that were removed and interpolated. Figure 4c shows the vertical component of the geophone dataset set after the interpolation. Figure 5 displays the first break times picked for the DAS and geophone data. An interesting observation is the change of the first break times after integration of the DAS data going from a peak to a zero crossing pick.

As mentioned earlier, eight source points were selected for particular discussion (Figure 2). The offset range is from 30 m to 200 m approximately increasing from the well at each side of the walk away line. Therefore, the following figures will focus on these selected source points.

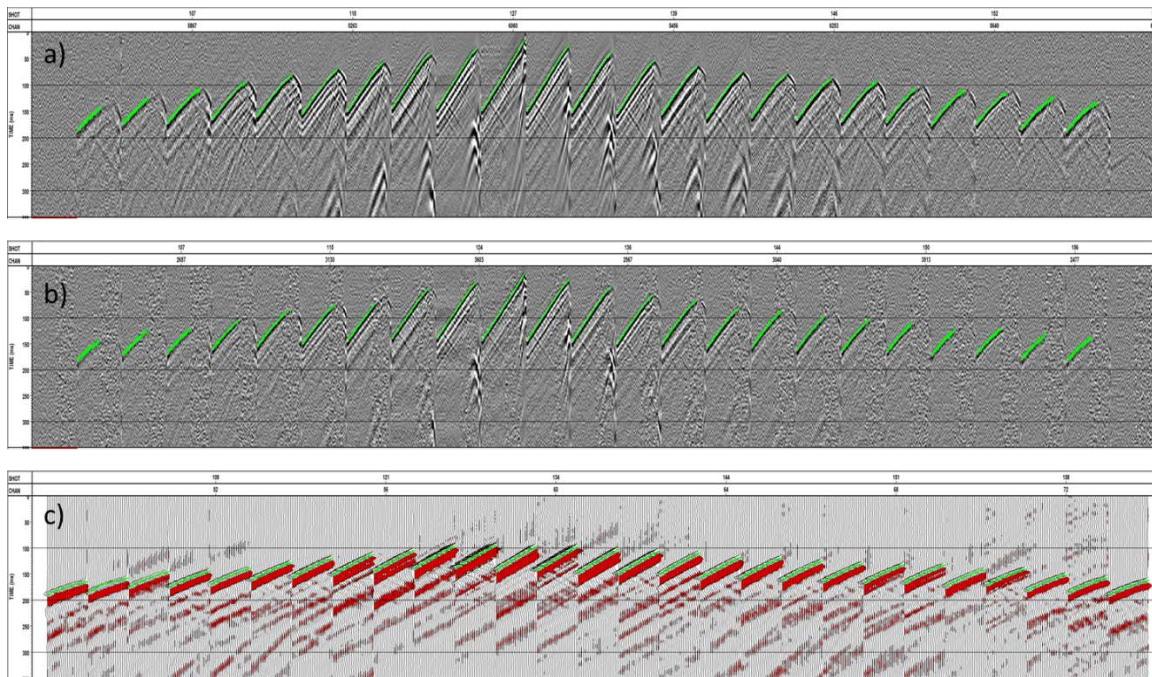


Figure 5. First break times shown in green. a) straight fibre, b) helical fibre and c) geophone vertical component.

Wavefield separation

A median filter was used to separate the downgoing and upgoing wavefields. For the DAS datasets, a median filter of 91 samples was applied which is equivalent to 22.75 m. The median filter applied to the geophones was of 5 samples or 25 m. In both cases, there is a good separation of the downgoing and upgoing waves. Nevertheless, the DAS data had various downgoing events remaining in the upgoing wavefield. Therefore, an F-K filter was also applied. Figures 6-17 show the downgoing and upgoing wavefield of the straight fibre, helical fibre and geophone vertical component and rotated data, respectively.

Prior the wavefield separation of the multicomponent geophone data, several processing steps were completed. The first step consisted on two data rotations through a hodogram analysis. The horizontal components (H1 and H2) were rotated to Hmax and Hmin where the Hmax is oriented in the well-source plane and Hmin is perpendicular (Hinds et al., 1996). The second rotation was applied to the vertical component (Z') and Hmax. The output Hmax' is oriented in the direction of the wave front thus is also known as radial component and contains downgoing events and upgoing SV. The second output of the rotation, the transversal component (Z') contains upgoing events product of the reflected waves. Following the geophone data rotation, a time variant polarization was also performed since the hodogram analysis assumes a constant angle of incidence. With this polarization, we assume the rotation angle changes with time. We use a ray-tracing model and a velocity model corresponding to a zero offset VSP. After this last rotation, we are obtain a more accurate wavefield separation from where upgoing P-waves and S-waves can be separated afterward. In this case, we encountered some difficulties with the ray-

tracing model building and for this reason the wavefield separation of the geophone vertical component seems to have a cleaner result.

After completing these steps of the processing, a good wavefield separation was obtained for each dataset. However, there are some upgoing events remaining in the DAS downgoing wavefields, especially for the farthest offsets of approximately 200 m from the well (Figures 6, 8, 10 and 12). Additionally, several downgoing S-wave events are also noticeable in both the straight and helical wound fibre that also seem to be more predominant as the offset increases. Overall, the upgoing wavefield has a good representation of the injection target, the Basal Belly River Sandstone with an approximate depth of 300 m (bright event in figures 7, 9, 11, 13, 15 and 17).

Raw DAS:

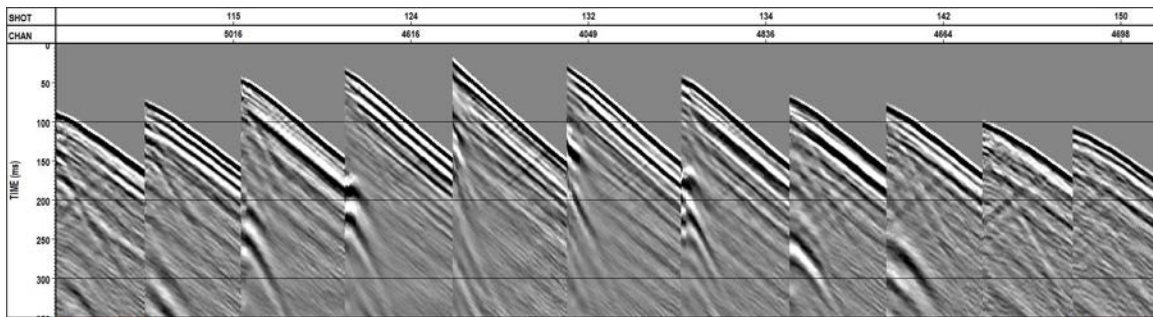


Figure 6. Downgoing wavefield of straight fibre.

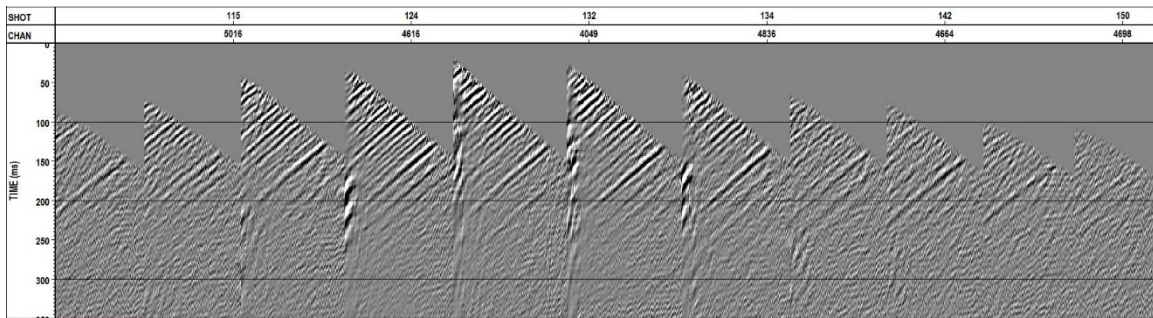


Figure 7. Upgoing wavefield of straight fibre.

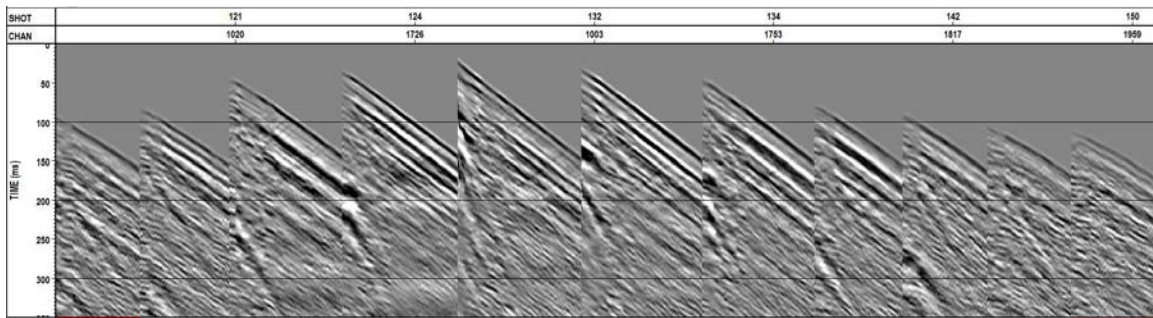


Figure 8. Downgoing wavefield of helical wound fibre.

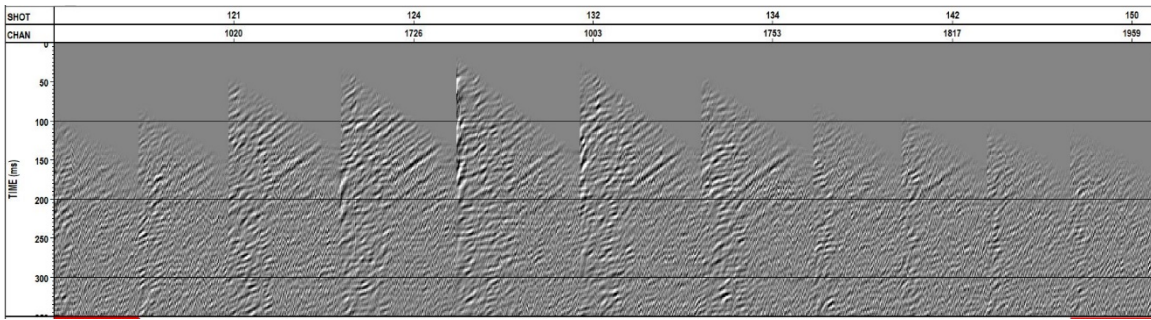


Figure 9. Upgoing wavefield of helical wound fibre.

Integrated DAS:

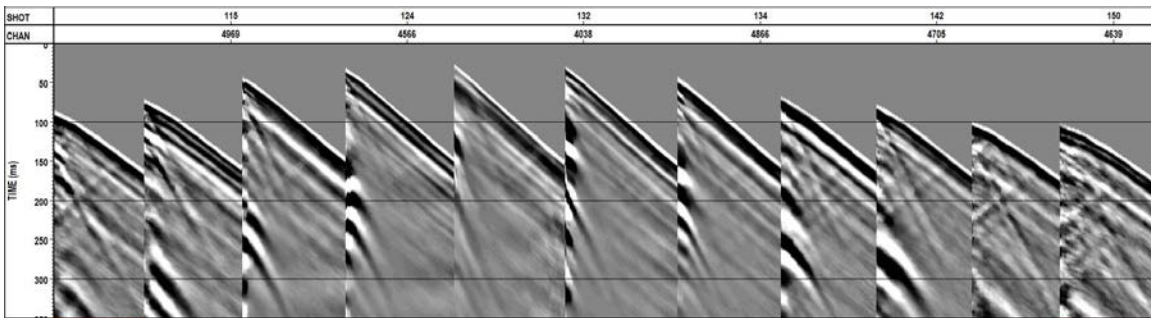


Figure 10. Downgoing wavefield of integrated straight fibre.

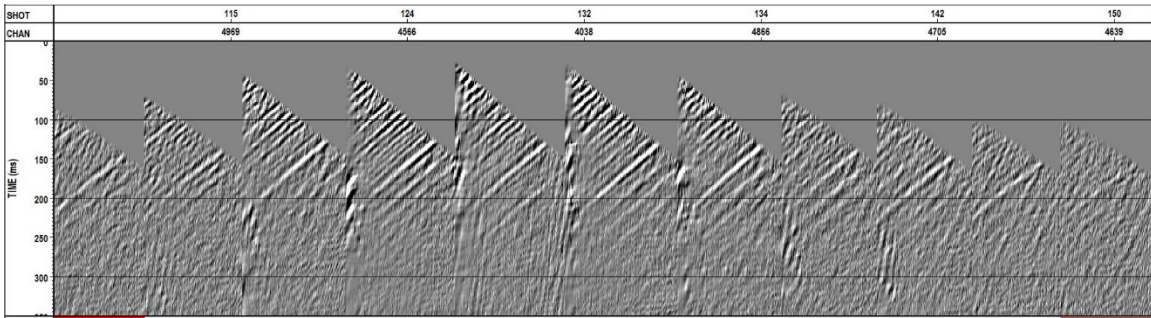


Figure 11. Upgoing wavefield of integrated straight fibre.

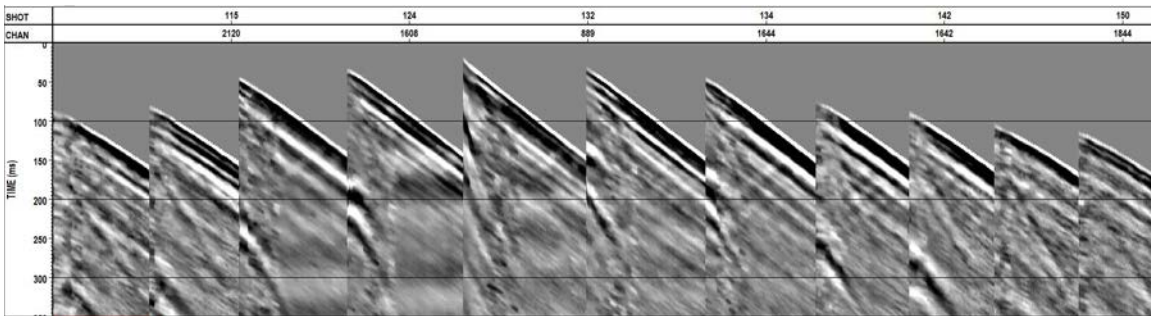


Figure 12. Downgoing wavefield of integrated helical wound fibre.

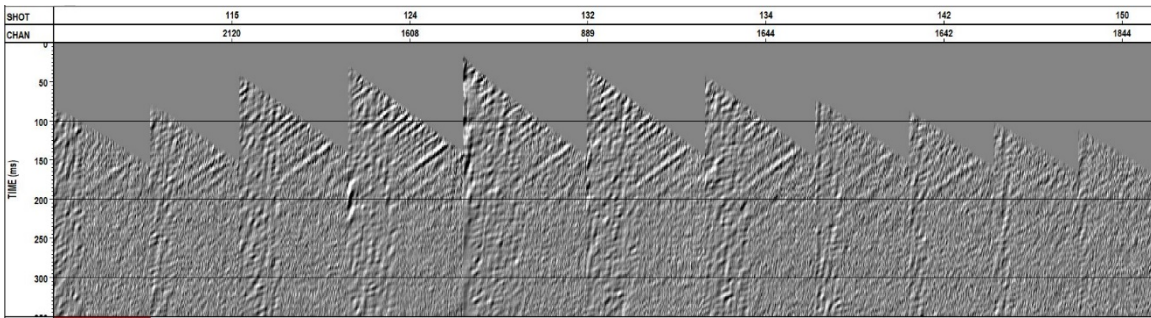


Figure 13. Upgoing wavefield of integrated helical wound fibre.

Geophones:

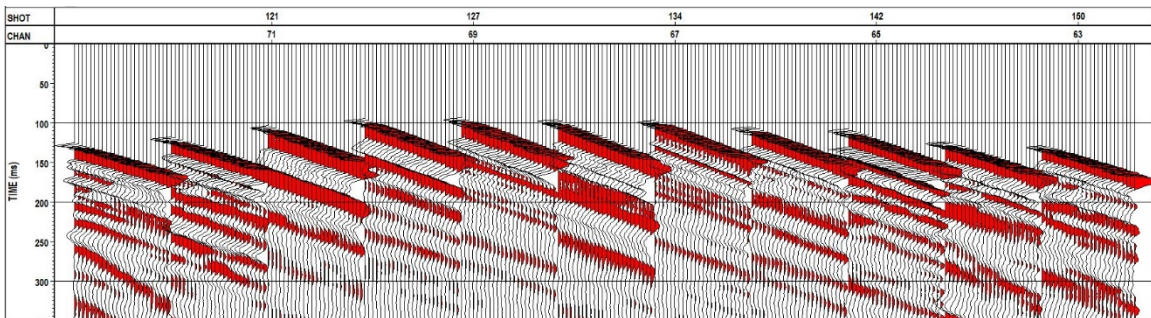


Figure 14. Downgoing wavefield of geophone array (vertical component).

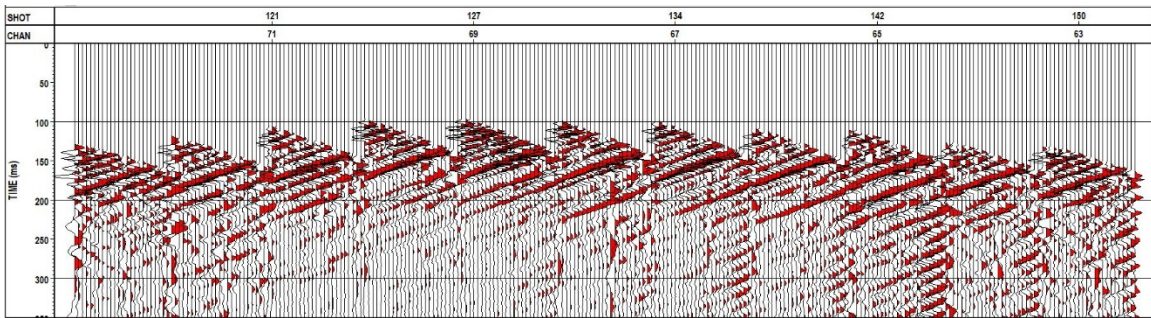


Figure 15. Upgoing wavefield of geophone array (vertical component).

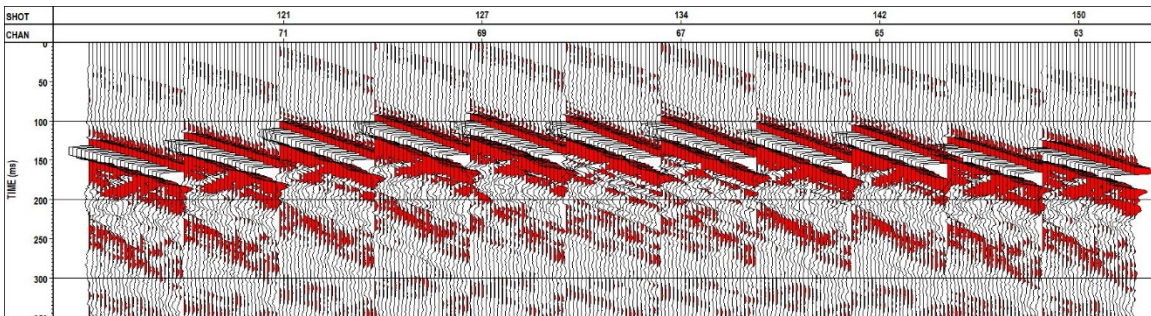


Figure 16. Downgoing wavefield of geophone array (rotated data).

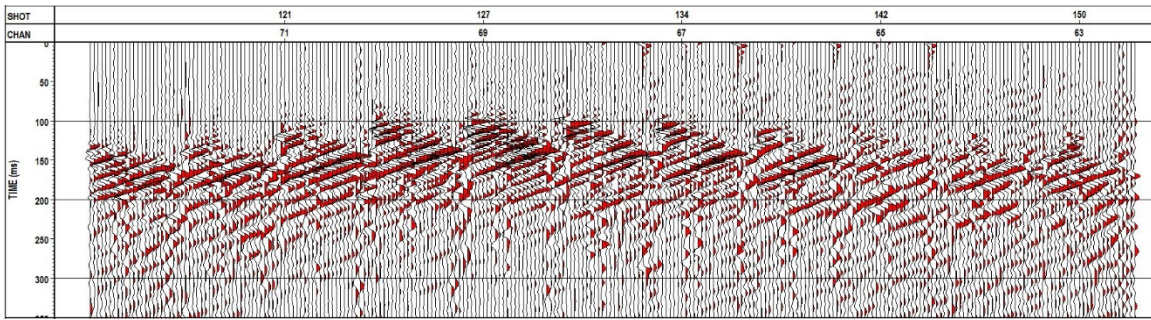


Figure 17 Upgoing wavefield of geophone array (rotated data).

Deconvolution operator

With the downgoing wavefield, a deconvolution operator was generated and then applied to the upgoing wavefield of each dataset with the objective to obtain a better definition of the events. As shown in Figures 18-29, after the deconvolution operator was applied, there is an improvement in the image in every dataset. The events seem sharper and continuous; however, the helical data shows a weaker response compared to the straight fibre, and any remaining noise in the data could overshadow the upgoing events.

Raw DAS:

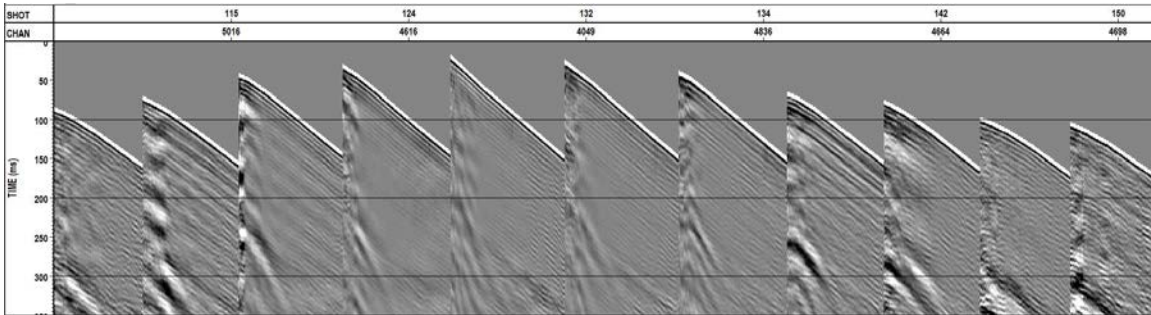


Figure 18. Downgoing wavefield after deconvolution of raw straight fibre.

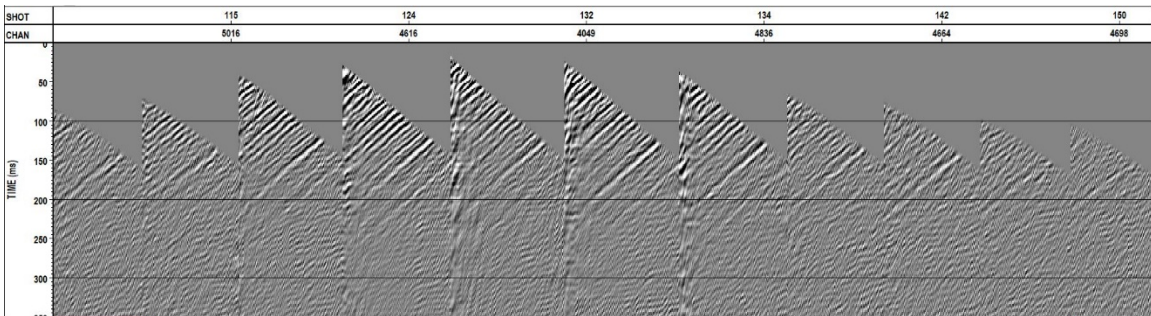


Figure 19. Upgoing wavefield after deconvolution of raw straight fibre.

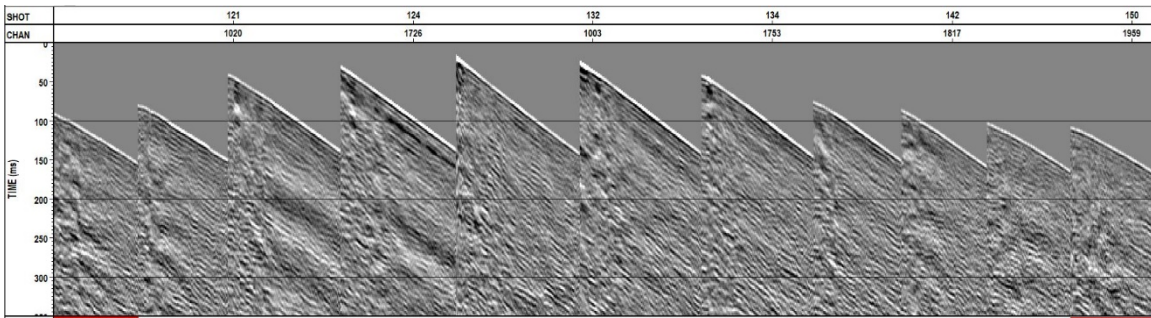


Figure 20. Downgoing wavefield after deconvolution of raw helical wound fibre.

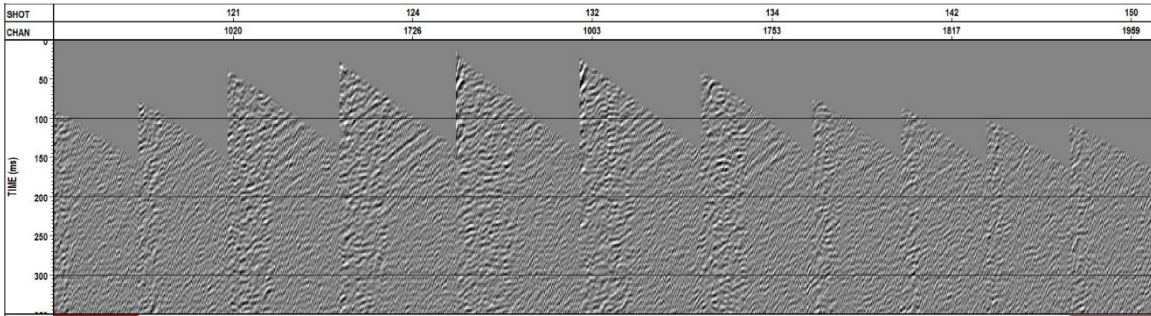


Figure 21. Upgoing wavefield after deconvolution of raw helical wound fibre.

Integrated DAS:

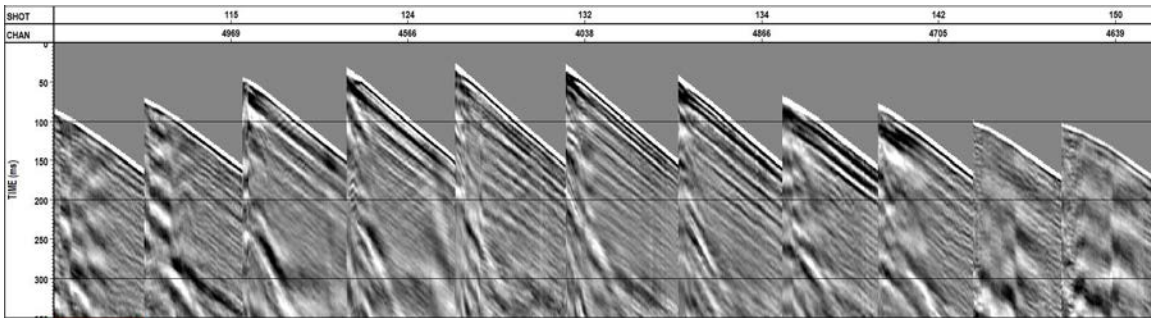


Figure 22. Downgoing wavefield after deconvolution of integrated straight fibre.

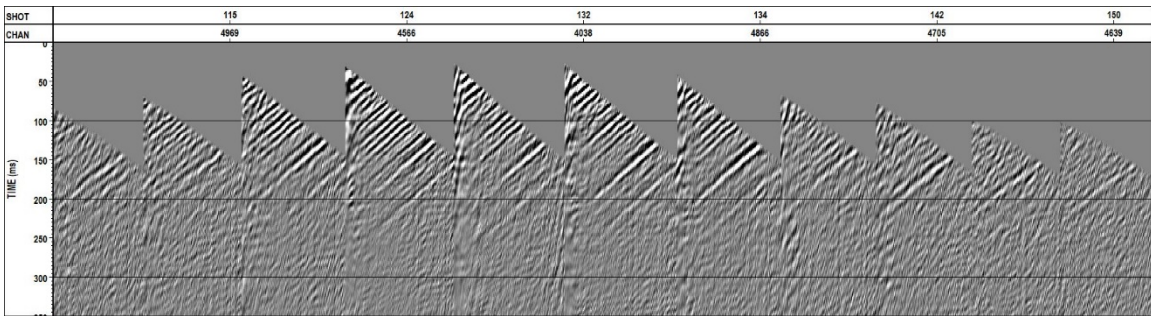


Figure 23. Upgoing wavefield after deconvolution of integrated straight fibre.

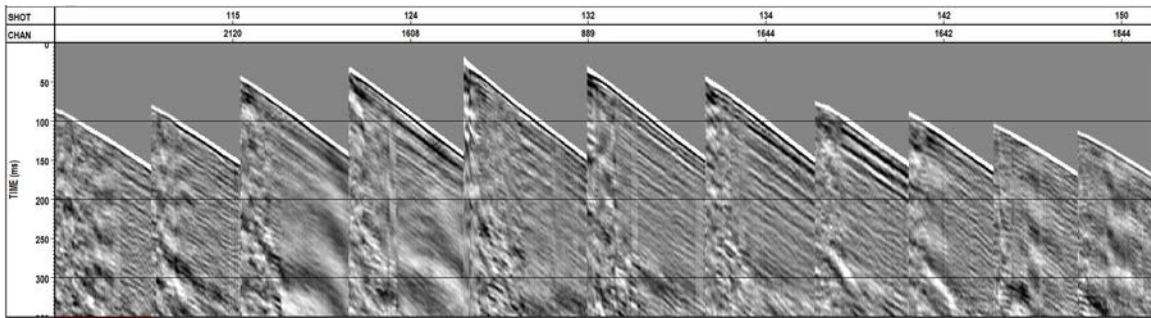


Figure 24. Downgoing wavefield after deconvolution of integrated helical wound fibre.

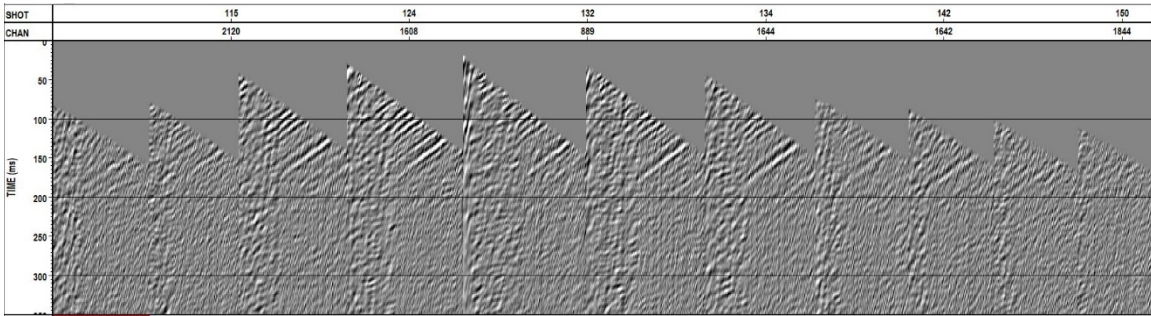


Figure 25. Upgoing wavefield after deconvolution of integrated helical wound fibre.

Geophones:

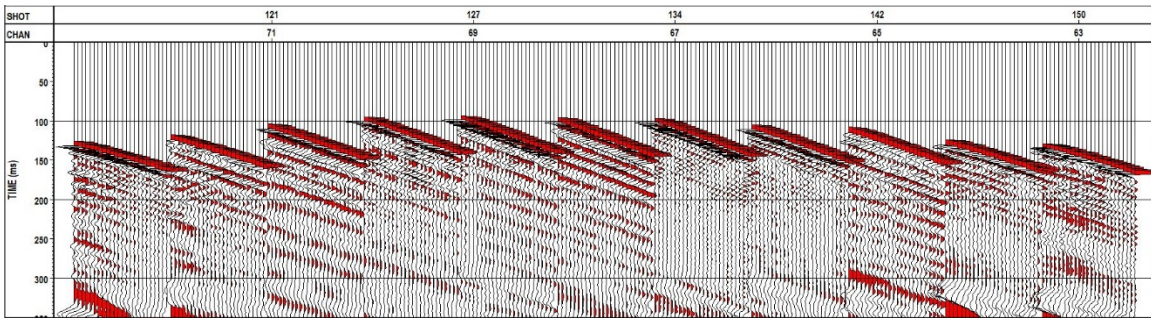


Figure 26. Downgoing wavefield after deconvolution of geophone array (vertical component).

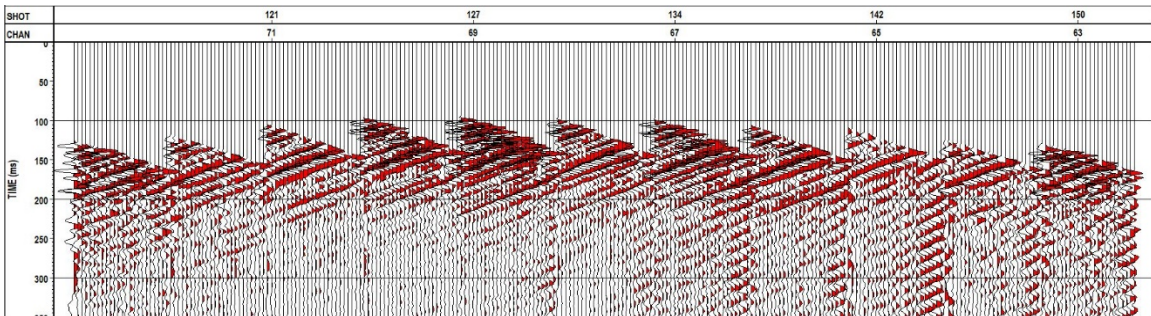


Figure 27. Upgoing wavefield after deconvolution of geophone array (vertical component).

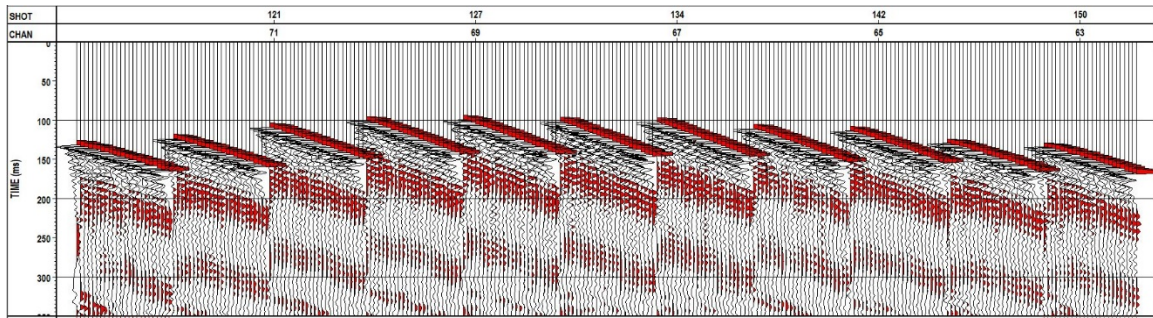


Figure 28. Downgoing wavefield after deconvolution of geophone array (rotated data).

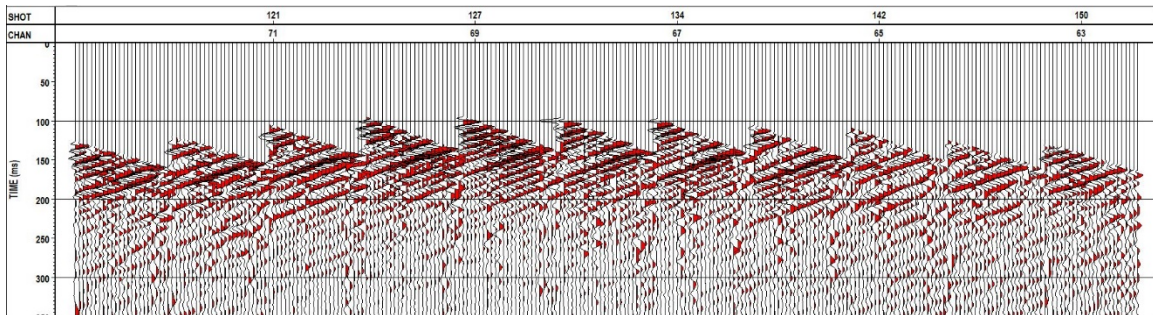


Figure 29. Upgoing wavefield after deconvolution of geophone array (rotated data).

VSP-CDP transform and stacking

The VSP-CDP transform is a mapping procedure that moves offset VSP data to their corresponding reflection point assuming a marginal dip (Sheriff, 2002). The mapping displays a coverage from the wellhead to the farthest reflection given by the velocity model available and the VSP geometry (Hinds et al., 1996). Among the parameters used for the VSP-CDP transform, firstly we used every 4 traces (0.25 m) from the DAS gathers as the large number of traces were slowing down the transform calculation. The trace spacing output selected for the DAS was of 1 m and 2.5 m for the geophones which is similar to the trace spacing of DAS after the data selection and half of the channel spacing for the geophones. The velocity models used for the transform were obtained from the first break arrivals of a zero offset VSP. The DAS velocity profile was smoothed to have a blocky trend, this was achieved with a 10 m spacing between samples (Figure 30).

The VSP-CDP transform was applied to eight source points at increasing offsets from the well varying from 30 m to 200 m approximately. These particular source points were selected to show a symmetric comparison at each side of the line and therefore have consistency during the analysis. The results obtained for each dataset are shown below (Figures 31-36) where there is a good event identification along the different offsets. The CO₂ injection target located at approximately 250 ms is noticeable in each dataset and offset. However, there is an apparent discontinuity of the event of interest across the mapped result, particularly for the raw fibre (Figures 31 and 32).

On the other hand, DAS datasets yield a better illumination in the shallow section due to the full coverage of the fibre in the well compared to the geophone coverage that is restricted to the zone of interest.

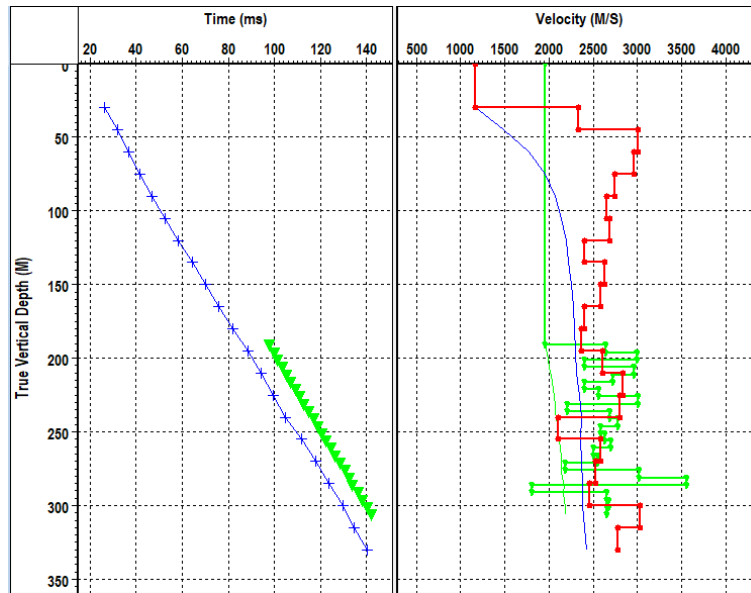


Figure 30. Interval velocity profile of zero offset VSP. Straight DAS (red) and geophone vertical component (green).

Raw DAS:

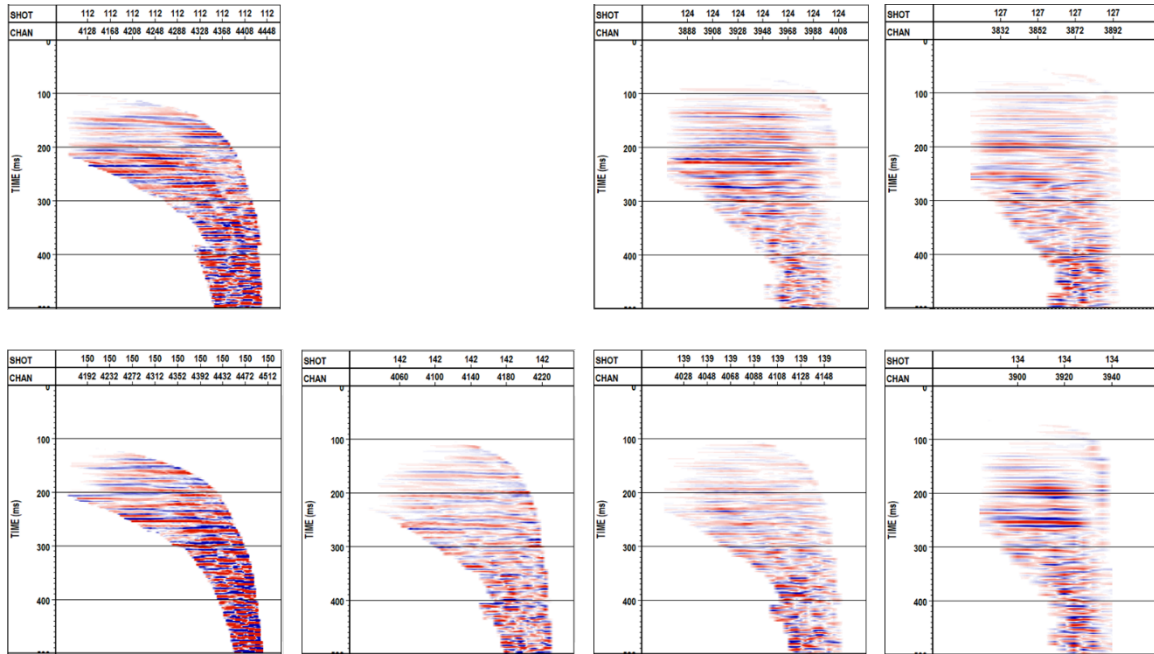


Figure 31. VSP-CDP transform of raw straight fibre at different offsets from the well.

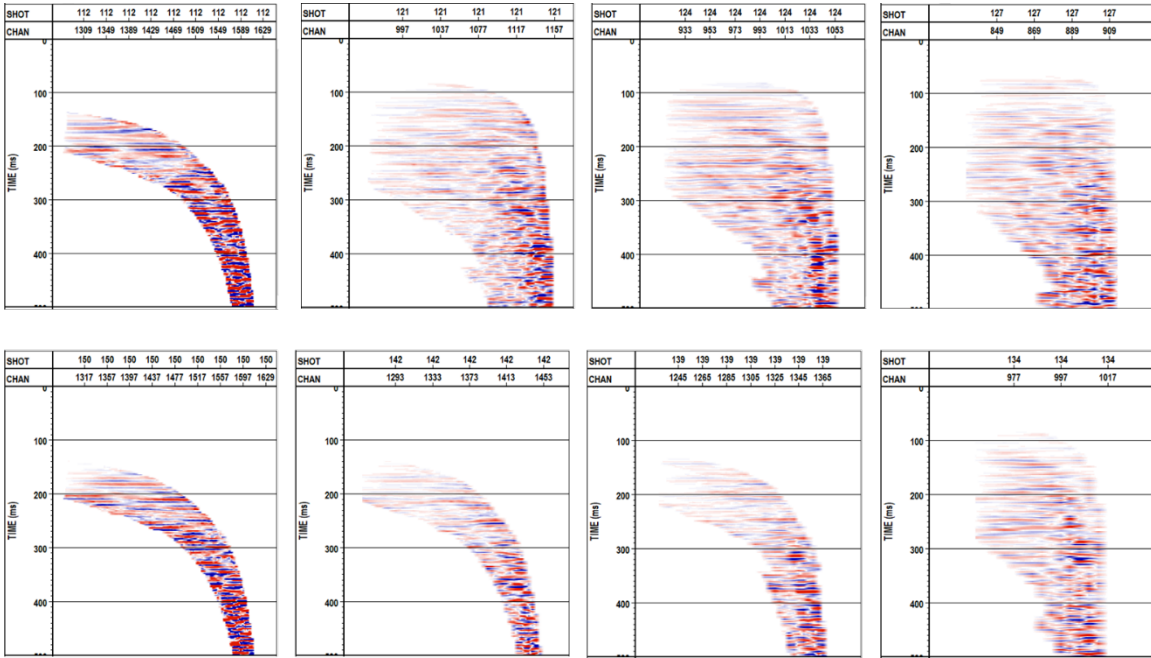


Figure 32. VSP-CDP transform of raw helical wound fibre at different offsets from the well.

Integrated DAS:

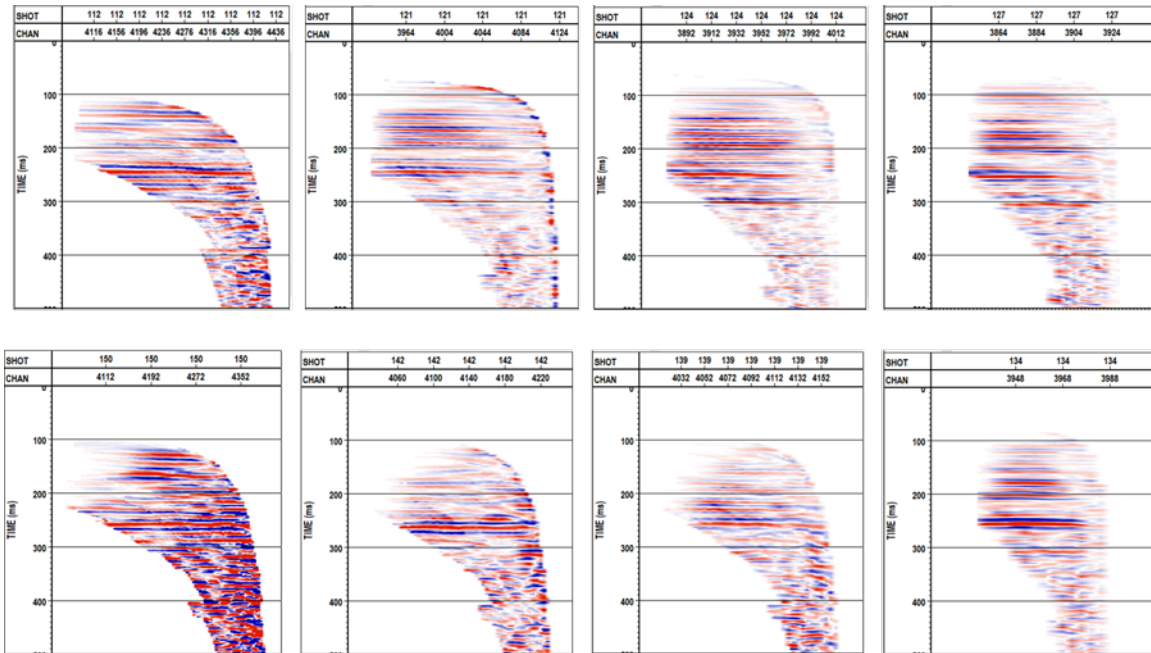


Figure 33. VSP-CDP transform of integrated straight fibre at different offsets from the well.

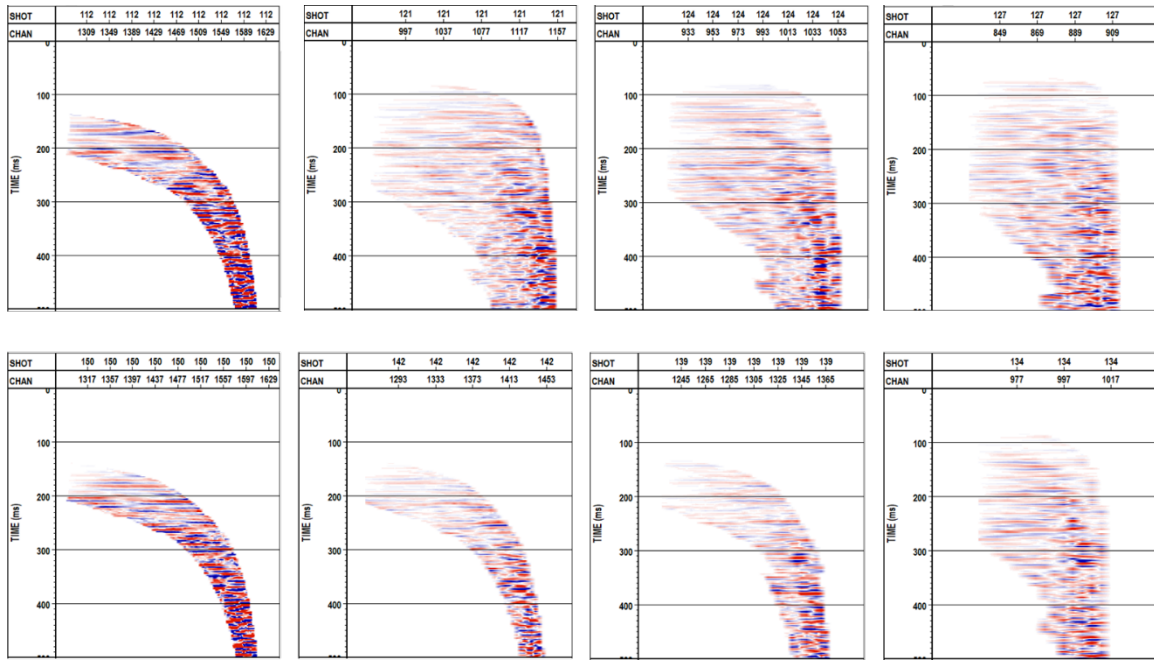


Figure 34. VSP-CDP transform of integrated helical wound fibre at different offsets from the well.

Geophones:

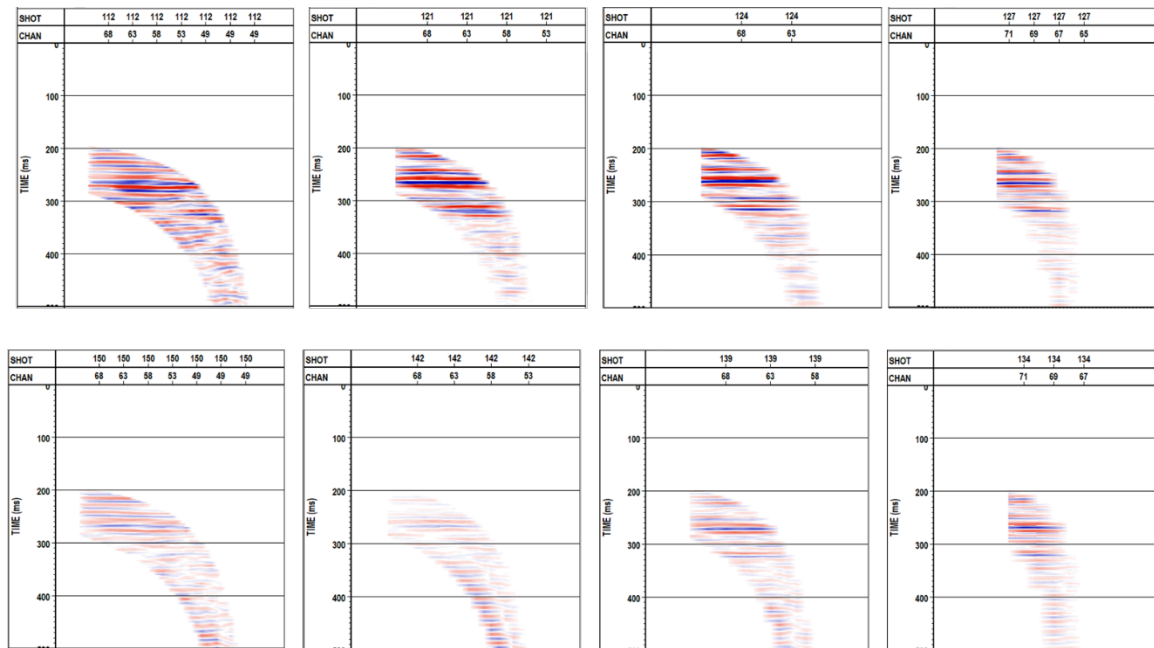


Figure 35. VSP-CDP transform of geophone array (vertical component) at different offsets from the well.

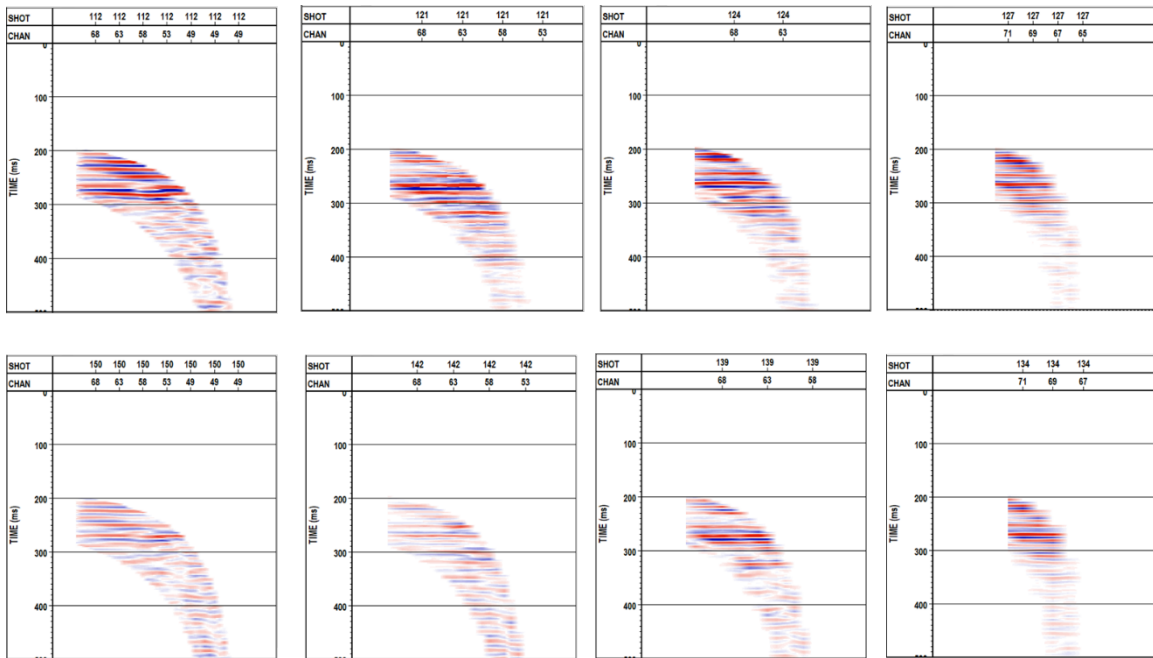


Figure 36. VSP-CDP transform of geophone array (after rotation) at different offsets from the well.

Stacking

Following the VSP-CDP transform, the data from each VP was stacked. Figures 37, 38 and 39 show the imaging result obtained from the source points selected earlier. In this case, we are showing the stacked DAS data side to side for a better visualize the differences between the straight and helical fibre results. Similarly, for the geophones with the vertical component and rotated data. In the three cases, the event of interest (250 ms) is noticeable and continuous along the majority of the section. However, for the helical dataset, the mapped image looks weaker compared to the straight fibre and the event of interest seems to have some discontinuity in the stacked sections.

Raw DAS:

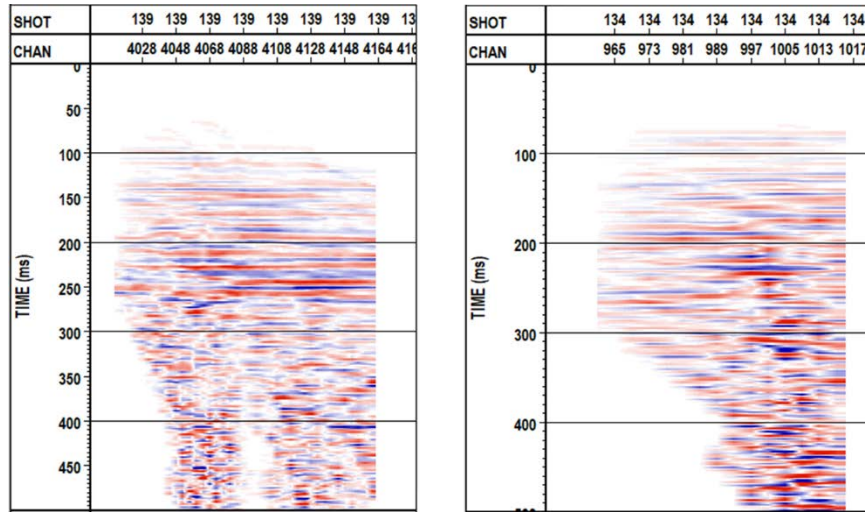


Figure 37. VSP-CDP stacks. Raw straight cable (left) and raw helical wound cable (right).

Integrated DAS:

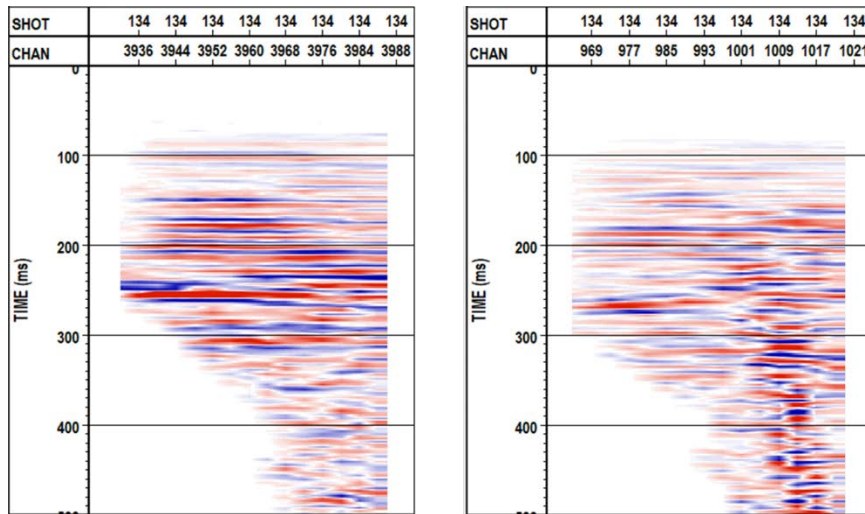


Figure 38. VSP-CDP stacks. Integrated straight cable (left) and integrated helical wound cable (right).

Geophones:

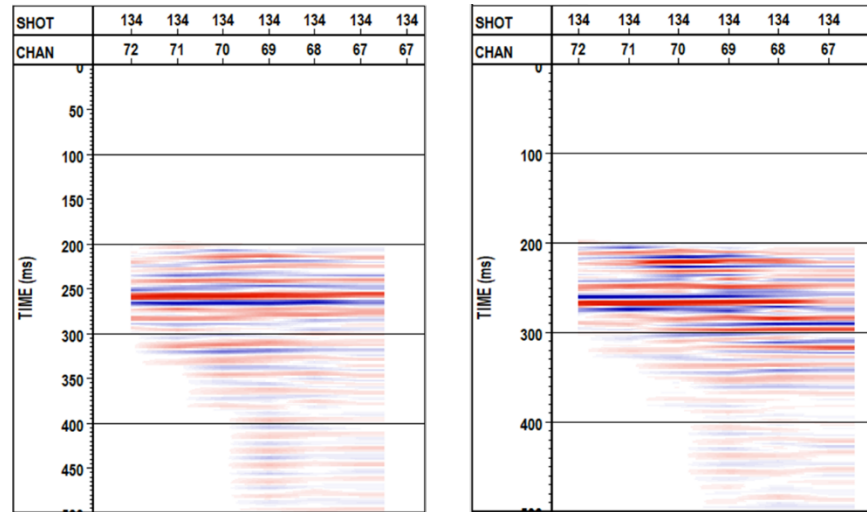


Figure 39. VSP-CDP stacks. Geophone vertical component (left) and geophone rotated data (right).

RESULTS DISCUSSION

After reviewing the results of each step in the processing flow, we have noticed several important remarks between the different datasets. For example, the raw straight DAS data seems less noisy than the helical DAS, this could be associated with the effect of the fibre configuration. The integrated DAS has better visualization of the seismic events compared to the raw DAS. The DAS data yields a broader illumination in the shallow section with respect to the geophones that were deployed across the injection zone. In the wavefield separation, we noticed the identification of head waves in DAS datasets again related to the full coverage of fibre in the well. As the offset increases, more S-wave events are present in the data which is normal due to the difference in the angle of incidence of the rays as they travel from the source to the receivers in the well. There is a good correlation between the upgoing events identified in both DAS and geophone datasets. After deconvolution, the events seem better defined and continuous, in particular for the helical DAS that showed weaker events as the offset increased. From the VSP-CDP transforms there is a good resemblance of the events for each data set, the event of interest is identified at every offset. The integrated DAS seems to have a more continuous correlation of the events and the geophone dataset has a subtler appearance with respect to DAS, which proves one of the advantages of this method, higher resolution data. Similarly, with the stacked sections, the injection target is visible and seems better defined in the integrated DAS.

The stacked sections were also compared with an inline of a 3D seismic survey acquired at the FRS in 2014 that crosses the observation well 2. Figures 40, 41 and 42 show comparison of sections from the processed surface seismic data with the raw DAS, integrated DAS and the geophones respectively. As mentioned before, straight DAS seems to have a better display of the target of interest compared to the helical fibre; this also applies for the raw and integrated sections where even though there is better continuity of

the events, the target in the helical section seems to vary in the stacked section. This could be associated to the increased signal sensitivity from the fibre configuration that would need further analysis.

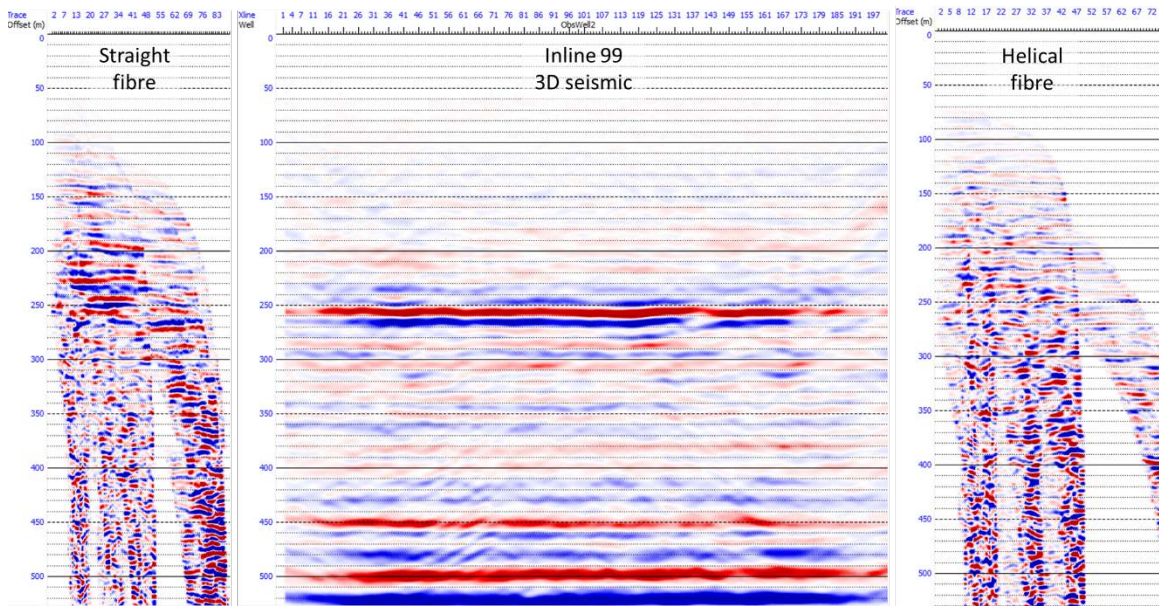


Figure 40. Raw DAS stacked section compared to surface seismic section. Straight fibre (left) and helical fibre (right).

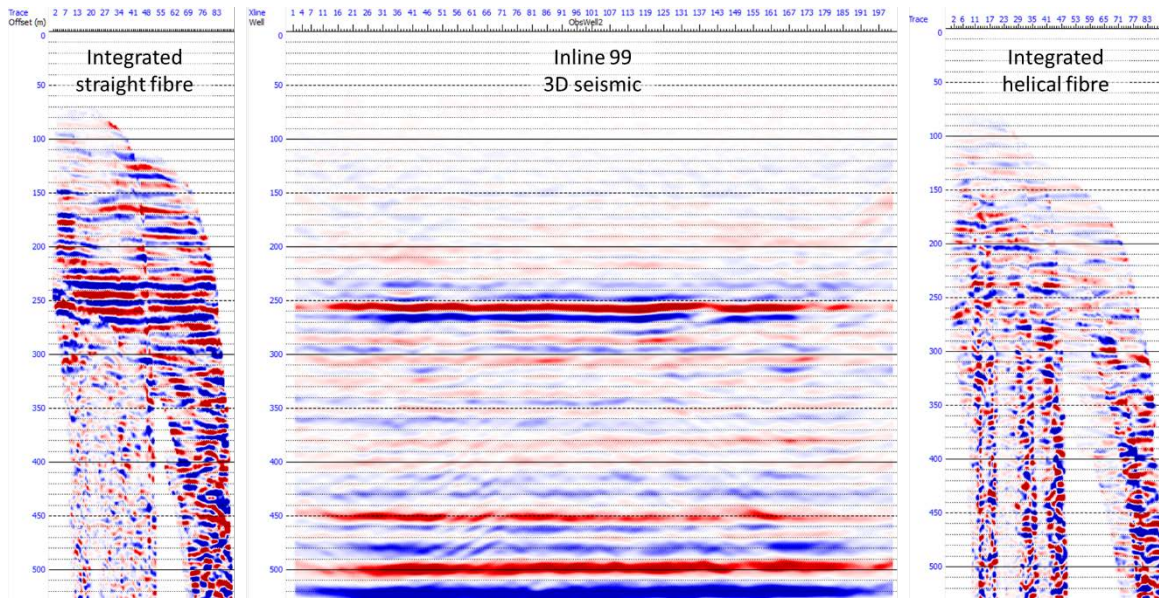


Figure 41. Integrated DAS stacked section compared to surface seismic section. Straight fibre (left) and helical fibre (right).

The geophone dataset shows a good correlation between the surface seismic and the stacked sections of the walk away VSP. The vertical component section yields flatter events compared to the rotated geophone data. This might be associated with remaining SV waves after the rotation and time-variant orientation.

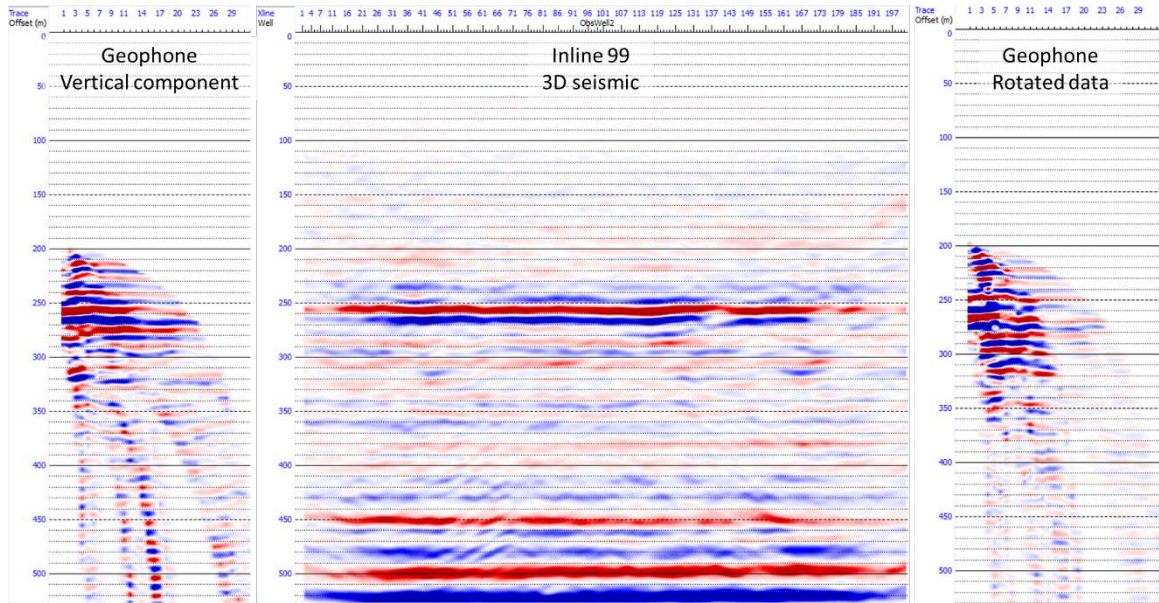


Figure 42. Geophone stacked section compared to surface seismic section. Geophones vertical component (left) and rotated geophone (right).

Overall, the three datasets that were processed (straight fibre, helical fibre and geophones) yield a good imaging result that can be correlated to surface seismic data. The event of interest was identified in each dataset and it also matched the surface seismic. DAS dataset also shows more seismic events in the shallow section that could be helpful for further studies of the overburden section.

CONCLUSIONS

A walk away VSP line acquired at the Field Research Station in July 2017 was processed while performing a thorough comparison between the DAS and geophone datasets. The analysis included the assessment of the straight and helical wound fibre optic cables as well as the geophones vertical component and multicomponent data. Additionally, the same procedure was applied to the integrated DAS datasets.

There is a good correlation between the DAS datasets and the geophone data. Having a full coverage of the fibre optic cables in the well yields better imaging results in the shallow section. A clear identification of the target was achieved for the raw and integrated straight fibre, although the results obtained for the helical fibre seem less continuous in the zone of interest.

The stacked sections also show a good correlation with an inline from a 3D surface survey passing through observation well 2. This comparison gives us a positive effect on DAS applications for subsurface imaging while encouraging us to continue with the study of DAS measurements in particular for the helical fibre.

FUTURE WORK

These results are a motivation to continue with the processing of walk away lines acquired recently at the FRS. This will allow us the completion of the baseline while continuing with the assessment of DAS technology by testing different interrogator units and analyzing their datasets along the processing flow.

ACKNOWLEDGEMENTS

We are grateful to the sponsors of CREWES and of the CaMI FRS JIP, and NSERC through grant CRDPJ 461179-13 for financial support. This research was also supported in part by the Canada First Research Excellence Fund.

REFERENCES

- Lawton, D. C., 2017, Monitoring technology innovation at the CaMI Field Research Station, Brooks, Alberta. Calgary: CMC.
- Hinds R., Anderson N. and Kuzmiski R., 1996, VSP Interpretive Processing: Theory and Practice. *Open File Publications No.3*. Society of Exploration Geophysicists.
- Mateeva A., Lopez J., Potters H., Mestayer J., Cox B., Kiyashchenko D., Wills P., Grandi S., Hornman K., Kuvshinov B., Berlang W., Yang Z. and Demoto R., 2014, Distributed acoustic sensing for reservoir monitoring with vertical seismic profiling. *Geophysical Prospecting*, 679-692.
- Parker T., Shatalin S. and Farhadiroushan M., 2014, Distributed Acoustic Sensing – a new tool for seismic applications. *First Break*, 61-69.
- Sheriff R., 2002, *Encyclopedic Dictionary of Applied Geophysics*.
- Wu H., Wong W., Yang Z., Wills P. B., Lopez J., Li Y., Blonk B., Hewett B. and Mateeva A., 2015, Dual-well 3D vertical seismic profile enabled by distributed acoustic. *Interpretation*, SW12--SW25.